

# Self-Guidance: Boosting Flow and Diffusion Generation on Their Own

Tiancheng Li<sup>1,2</sup> Weijian Luo<sup>1,3,\*</sup> Zhiyang Chen<sup>1,4</sup> Liyuan Ma<sup>1,4</sup> Guo-Jun Qi<sup>1,4,\*</sup>

<sup>1</sup>MAPLE Lab, Westlake University, <sup>2</sup>Zhejiang University, <sup>3</sup>Peking University

<sup>4</sup>Institute of Advanced Technology, Westlake Institute for Advanced Study

{litiancheng, chenzyang, maliyuan}@westlake.edu.cn

luoweijian@stu.pku.edu.cn, guojunq@gmail.com

## Abstract

*Proper guidance strategies are essential to achieve high-quality generation results without retraining diffusion and flow-based text-to-image models. Existing guidance either requires specific training or strong inductive biases of diffusion model networks, potentially limiting their applications. Motivated by the observation that artifact outliers can be detected by a significant decline in the density from a noisier to a cleaner noise level, we propose Self-Guidance (SG), which improves the image quality by suppressing the generation of low-quality samples. SG only relies on the sampling probabilities of its own diffusion model at different noise levels with no need of any guidance-specific training. This makes it flexible to be used in a plug-and-play manner with other sampling algorithms. We also introduce a more efficient approximation of SG, named SG-prev, which reuses the output from the immediately previous diffusion step to avoid doubling sampling time. We conduct experiments on text-to-image and text-to-video generation with different architectures, including UNet and transformer models. With open-sourced diffusion models such as Stable Diffusion 3.5 and FLUX, SG exceeds existing algorithms on multiple metrics, including both FID and Human Preference Score. SG-prev also achieves strong results over both the baseline and the SG with only one forward pass. Moreover, we find that SG and SG-prev both have a surprisingly positive effect on the generation of physiologically correct human body structures such as hands, faces, and arms, showing their ability of eliminating human body artifacts with minimal efforts. We will release our code along with this paper.*

## 1. Introduction

Over the past decade, deep generative models have achieved remarkable advancements across various applications [5, 6,

This project was initiated and supported by MAPLE Lab at Westlake University.

\* Corresponding author.

9, 14, 17, 21, 22, 25, 26, 36–38, 40, 42, 44, 45, 48]. Among them, diffusion models [12, 58, 60] and flow-based models [2, 8, 29] have notably excelled in producing high-resolution, text-driven data such as images [50, 51, 54], videos [4, 14, 67], and others [7, 20, 28, 39, 45, 56, 62, 68], pushing the boundaries of Artificial Intelligence Generated Contents.

In simple terms, diffusion models learn a multi-step transition from a prior distribution  $p_T(x_T)$  to a real data distribution  $p_0(x_0)$ . However, default sampling methods for diffusion and flow-based models often lead to unsatisfactory generation quality, such as **broken human hands and faces, and images with bad foreground and background**. To address these issues, various guidance strategies have emerged as cheap yet effective ways to guide the generation process for better generation quality. For instance, classifier-free guidance (CFG) [11] modifies the velocity of diffusion and flow-based generative models by adding a delta term between class-conditional and unconditional velocities, which pushes generated samples to have high class probabilities.

Though these existing guidance have shown impressive performance improvements, they have various individual restrictions. For instance, the CFG relies on **computing an additional unconditional velocity**, which requires training the diffusion model under both conditional and unconditional settings, therefore, harms the modeling performances[1]. Auto-Guidance (AG) pays a significant price that requires training an additional *bad-version* model, which is **tricky as well as requiring more memory costs**. Other guidance, such as Perturbed-attention Guidance (PAG [1]), and self-attention guidance (SAG [16]), do not rely on additional training. However, as the PAG paper described, **the effectiveness of PAG is highly sensitive to the selection of perturbed attention layers** inside the neural network, making it less flexible to enhance models in general applications. We notice that *all these guidance variants focus on diffusion sampling strategies at a single timestep, while neglecting how diffusion sampling at various timesteps could be explored to improve the generation quality*. Furthermore, we find that without explicitly retraining or perturbing an exist-

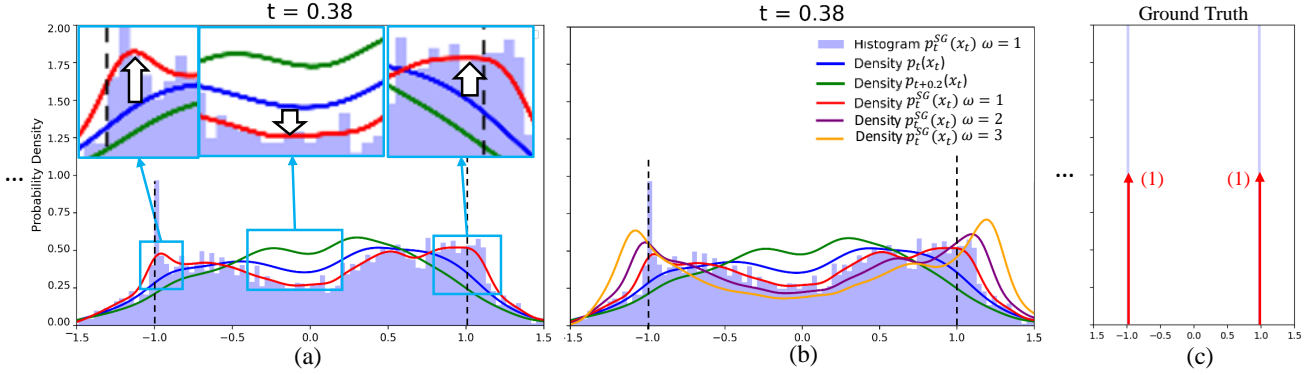


Figure 1. We train a diffusion model on a 1-dimensional toy example with data drawn from two separate modes at  $\pm 1$ . At different noise levels  $t$ , we fit and plot the distribution of generated samples in the reverse diffusion process. (a) The results on diffusion time  $t = 0.38$ . The blue curve plots the distribution of generated samples at the current noise level  $t$ , while the green curve plots the distribution of samples generated at the noisier level  $t + \delta(t)$ . The red curve shows the obtained SG sampling distribution after applying the ratio of these two probabilities with  $\omega = 1$ . (b) With various  $\omega$ , we show that artifact samples around the origin are suppressed more sharply with a larger value of  $\omega$ , while the density of samples around two groundtruth modes is boosted. (c) The groundtruth two-mode distribution at  $\pm 1$ .

ing diffusion model as in CFG and PAG, using the diffusion samplings from different timesteps yields a Self-Guidance (SG) approach.

Specifically, for a diffusion model, we find that the reason for generating unnatural images is due to the inadequate denoising that could yield artifacts in the reverse diffusion process. As Figure 1 shows, let us consider a simple diffusion model trained on a 1-dimensional toy dataset with two separate modes at  $\pm 1$  as the ground truth. At the noise level  $t = 0.38$  for example, the probability  $p_t(x_t)$  (i.e., the blue curve) is likely to draw artifact samples around the origin as it has a large density at  $x_t = 0$ .

To relieve it, an intuitive idea is to take a look at the diffused probability  $p_{t+\delta(t)}(x_t)$  at a noisier level  $t + \delta(t)$  (i.e., the green curve). We know that the samples at this level could be noisier and thus contain more severe artifacts. Therefore, by comparing between these two levels, one can assume that if the density at the **cleaner** level  $t$  (although it is still high) declines significantly from that at the **noisier** level  $t + \delta(t)$ , the corresponding samples are likely to be artifacts, since the belief of sampling them as cleaner outputs has greatly dropped as reflected by the declining density. This is what we have seen in Figure 1(a)-(b), where the current sampling probability  $p_t(x_t)$  of the blue curve at  $t = 0.38$  declines from that of the green curve at the noisier level  $t + 0.2$  at the origin. This reveals that the samples around the origin could be artifacts, which is true. This decline can be measured by the ratio of these two probabilities, resulting in a new sampling strategy with

$$p_t^{SG}(x_t) \propto p_t(x_t) \left\{ \frac{p_t(x_t)}{p_{t+\delta(t)}(x_t)} \right\}^\omega, \quad (1.1)$$

to guide the reverse diffusion process. Here,  $\omega$  is the guidance scale. The higher the value of  $\omega$ , the more sharply the

artifact samples will be suppressed as shown in Figure 1(b).

In this paper, we present such an inference-time sampling strategy called *Self-Guidance (SG)* since it only involves its own diffusion model at different noise levels. For image generation tasks, as shown in Fig. 2, compared with the benchmark diffusion sampling algorithm, applying Self-Guidance successfully removes unwanted artifacts in generated images, fixing errors on human fingers and other generation errors, eliminating irrelevant objects, and improving text-image consistency.

This guidance can further be approximated using the output from the immediately previous diffusion step – i.e.,  $p_{t+1}(x_{t+1})$ . We denote this approximation as *SG-prev*. SG-prev only needs one forward pass, thereby incurring no additional inference cost and keeping the overall inference time almost unchanged.

In addition, SG is architecture-independent and can therefore be integrated into almost all existing diffusion and flow-based models regardless of varying model architectures. Unlike CFG [11] and AG [23], SG does not require additional guidance-specific training. SG is orthogonal to many other guidance approaches [1, 11, 23], and it can seamlessly work together with them in a plug-and-play manner for better performances.

In Section 5.2, we apply SG and SG-prev on Flux.1-dev [29] and Stable-Diffusion 3.5 [8, 52], as well as a representative text-to-video model, CogVideoX[67]. We show that when using SG only, all models achieved improved FID [10] and higher human preference scores on the HPS v2.1[64] benchmark. Combining SG and SG-prev with other established guidance methods, including CFG and PAG, leading to new state-of-the-art diffusion generation results, achieving 20.74 on FID, 31.56 on HPSv2, and 5.7845 on Aesthetic Score. Experiments on text-to-video generation also confirm



Figure 2. **Qualitative comparisons between Flux.1 (baseline) and Self-Guidance (SG) diffusion samples.** We compare the generated images of Flux and our SG from four parts. The red box in the figure represents the bad Flux generation and the better SG generation, and the enlarged image is shown in the lower right corner.

the solid performance improvements brought by SG.

The main contributions of this work are as follows.

- We observe that the ratio of probabilities at different noise levels serves as a good indicator of artifacts during the reverse diffusion process.
- Leveraging this insight, we propose *Self-Guidance*—a plug-and-play guidance method that improves generation quality without requiring extra training, supervision, or external models. Moreover, such guidance can be implemented without incurring additional inference cost, using a variant we refer to as SG-prev.
- We show that SG and SG-prev are compatible with other sampling methods like CFG and PAG, leading to state-of-the-art image generation performances.

## 2. Related Works

There are roughly two kinds of diffusion guidance. The first kind mixes the outputs of multiple models to get the generative velocity. The classifier-free guidance (CFG) [11] uses

a mix of conditional and unconditional score functions as the velocity. Most recently, the Auto-guidance (AG) [23] proposed to mix the current score output with a *bad-version* model to enhance persistence of velocity, resulting in improved performances. Both CFG and AG use two models for inference explicitly or implicitly. Some other studies have also elaborately studied guidance through the lens of diffusion solvers [33, 35, 66].

The second line of guidance defines the velocity by mixing the output of the score functions of a perturbed and the original sample. These methods usually need one model for inference. The self-attention guidance (SAG) [16] proposed to assign Gaussian perturbations to samples for guidance. Recently, Perturbed-attention guidance (PAG) [1] found that modifying the self-attention map of the diffusion model network for guidance results in strong performances. PAG-like guidance has shown steady improvements. Another recent work [53] proposed the TimeStep Guidance (TSG), which perturbed the timestep embedding of diffusion models, shar-

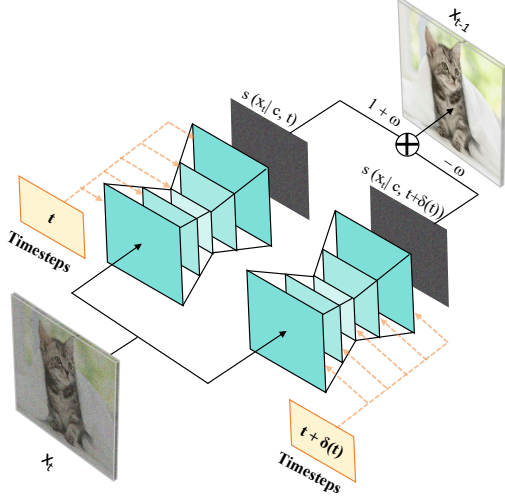


Figure 3. An illustration of Self-Guidance of one iteration step during generation.

ing a similar spirit as PAG. For perturbation-based guidance, how to choose proper perturbations is mostly decided in an ad-hoc manner, which may vary significantly across different neural network architectures. Other works also study perturbation-based guidance paradigms from different perspectives [3, 15, 41]. Despite improvements in overall image structure and class-label alignment, **existing guidelines have a common problem: they still generate images with artifacts**, like six-finger hands or twisted human bodies, which brings significant concerns in AI safety and user experiences. As a comparison, our proposed **Self-Guidance significantly improves fine-grained details of generated images, completing weaknesses of existing guidance in an orthogonal way**. We will introduce details of SG in Section 4.

### 3. Preliminary

**Diffusion Models** In this section, we introduce preliminary knowledge and notations about diffusion models [13, 57, 59]. The flow models [32, 34] share similar concepts that we put in the Appendix B. Assume we observe data from the underlying distribution  $q_d(x)$ . The goal of generative modeling is to train models to generate new samples  $x \sim q_d(x)$ . The forward diffusion process of DM transforms  $q_0 = q_d$  towards some simple noise distribution,

$$d\mathbf{x}_t = \mathbf{F}(\mathbf{x}_t, t)dt + G(t)d\mathbf{w}_t, \quad (3.1)$$

where  $\mathbf{F}$  is a pre-defined drift function,  $G(t)$  is a pre-defined scalar-value diffusion coefficient, and  $\mathbf{w}_t$  denotes an independent Wiener process. A continuous-indexed score network  $s_\varphi(\mathbf{x}, t)$  is employed to approximate marginal score functions of the forward diffusion process (3.1). The learning of score networks is achieved by minimizing a weighted

denoising score matching objective [59, 61],

$$\mathcal{L}_{DSM}(\varphi) = \int_{t=0}^T \lambda(t) \mathbb{E}_{\mathbf{x}_0 \sim q_0, \mathbf{x}_t | \mathbf{x}_0 \sim q_t(\mathbf{x}_t | \mathbf{x}_0)} \|\mathbf{s}_\varphi(\mathbf{x}_t, t) - \nabla_{\mathbf{x}_t} \log q_t(\mathbf{x}_t | \mathbf{x}_0)\|_2^2 dt. \quad (3.2)$$

Here the weighting function  $\lambda(t)$  controls the importance of the learning at different time levels and  $q_t(\mathbf{x}_t | \mathbf{x}_0)$  denotes the conditional transition of the forward diffusion (3.1). After training, the score network  $s_\varphi(\mathbf{x}_t, t) \approx \nabla_{\mathbf{x}_t} \log q_t(\mathbf{x}_t)$  is a good approximation of the marginal score function of the diffused data distribution. High-quality samples from a DM can be drawn by simulating generative SDE (3.3) which is implemented by replacing the score function  $\nabla_{\mathbf{x}_t} \log q_t(\mathbf{x}_t)$  with the learned score network [59].

$$d\mathbf{x}_t = \left\{ \mathbf{F}(\mathbf{x}_t, t) - \frac{1 + \tau(t)^2}{2} G^2(t) \mathbf{s}_\varphi(\mathbf{x}_t, t) \right\} dt + \tau(t) G(t) d\bar{\mathbf{w}}_t, \quad t \in [0, T], \quad \mathbf{x}_T \sim p_T. \quad (3.3)$$

**Classifier-free Guidance.** Though the diffusion model has a solid theoretical interpretation, directly using its score functions to simulate the generative SDE often leads to sub-optimal performances, especially for class-conditioned generation. Assume  $c$  is a class label, and  $s_\varphi(\mathbf{x}_t, t|c)$  is a conditional score network. The pioneering work Ho and Salimans [11] introduces the classifier-free guidance (CFG), which replaces the vanilla probability  $q_t(\mathbf{x}_t|c)$  with a new one  $\tilde{q}_t(\mathbf{x}_t|c) := q_t(\mathbf{x}_t) \left( \frac{q_t(\mathbf{x}_t|c)}{q_t(\mathbf{x}_t)} \right)^\omega$ .  $q_t(\mathbf{x}_t)$  represents the unconditional distribution which can be implemented by inputting an empty label  $\emptyset$  as  $q_t(\mathbf{x}_t|\emptyset)$ . With this, the new score function turns to

$$\tilde{s}_\varphi(\mathbf{x}_t, t|c) := s_\varphi(\mathbf{x}_t, t|\emptyset) + \omega \{s_\varphi(\mathbf{x}_t, t|c) - s_\varphi(\mathbf{x}_t, t|\emptyset)\} \quad (3.4)$$

Such a guidance strategy has become a default setting for diffusion models, such as the Stable Diffusion series [52]. However, the CFG strategy has its limitations. First, CFG requires both a conditional and an unconditional score network, which either requires two separate models or is challenging to train with a single model. Second, the CFG is not available for tasks such as purely unconditional generation.

### 4. Self-Guidance

Figure 1 demonstrates that using the ratio  $\frac{p_t(\mathbf{x}_t)}{p_{t+\delta(t)}(\mathbf{x}_t)}$  helps suppress artifacts arising from the original diffused probability  $p_t(\mathbf{x}_t)$  at each noise level  $t$ .

Formally, when generating the image with a condition  $c$ , the self-guided generative distribution at noise level  $t$  can be formulated as discussed in Section 1,

$$p_t^{SG}(\mathbf{x}_t|c, t) \propto p_t(\mathbf{x}_t|c) \left\{ \frac{p_t(\mathbf{x}_t|c)}{p_{t+\delta(t)}(\mathbf{x}_t|c)} \right\}^\omega. \quad (4.1)$$

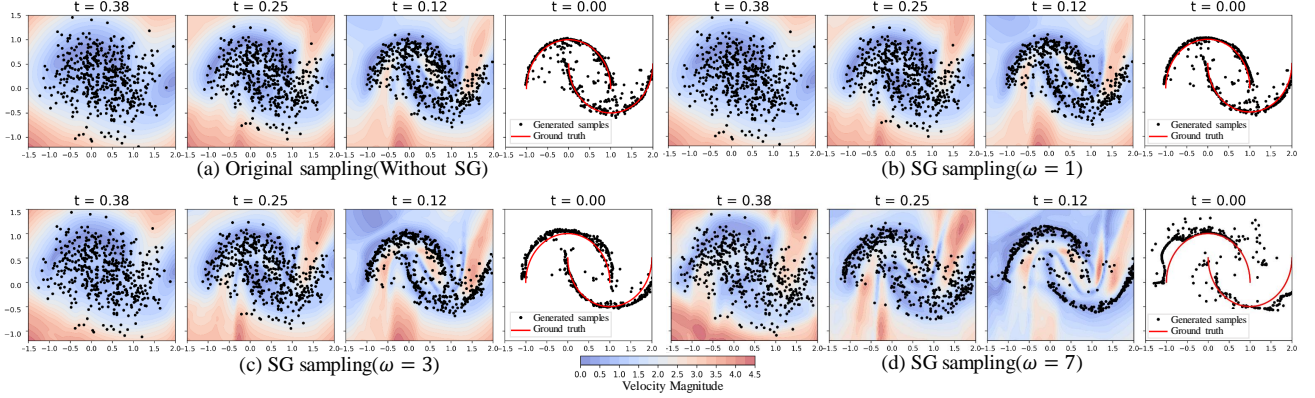


Figure 4. We train a flow-based diffusion model on a two-dimensional example with data sampled from a double-swirl pattern. We plot the distribution of the generated samples at the last four noise levels. The heat map in (a) shows the magnitude of predicted velocity without self-guidance, while the subfigures (b), (c), and (d) show those with Self-Guidance with various  $\omega$  and noise levels. With a larger  $\omega$ , more artifact outliers are successfully removed. Meanwhile, a too large value of  $\omega$  (e.g.,  $\omega = 7$ ) could underweight (or in other words, oversuppress) the sampling from the original density  $p_t(\mathbf{x}_t|\mathbf{c})$  that covers the swirl distribution. Thus, a suitable value of guidance scale is necessary to balance the sampling coverage and the artifact suppression.

This probability contains two parts. One is the original probability  $p_t(\mathbf{x}_t|\mathbf{c})$  that contains both the desired and artifact samples. The other is the ratio between probabilities of two diffusion times and it is used to suppress the artifacts. The guidance scale  $\omega$  acts as the combination weight.

Figure 1 has already illustrated the influence of  $\omega$  on the Self-Guidance sampling. Here we provide a more complex 2-dimensional example in Figure 4 to show the effects of Self-Guidance with various values of  $\omega$ . The groundtruth data are sampled from a double-swirl pattern. By comparing the diffusion samplings with and without Self-Guidance, it demonstrates the ability of SG to remove the artifact outliers that do not reside on the swirls. With an increasing value of  $\omega$ , the outlier artifacts are suppressed more sharply, which eventually leads to the high quality sampling of the groundtruth distribution. However, it is worth noting that when  $\omega$  becomes too larger (e.g.,  $\omega = 7$ ), the distribution of generated samples could start drifting away from the swirls. This is not surprising because too large  $\omega$  could underweight the original density  $p_t(\mathbf{x}_t|\mathbf{c})$  that aims to cover the samplings of the swirl data. This shows that a suitable guidance scale  $\omega$  is necessary to balance between the sampling of true data density and the suppression of artifact outliers. In experiments, we will study the effect of its choices in the ablation.

Since diffusion models output the score instead of the diffused probability, one can transform Eq. 4.2 into the score function by the relation of  $\mathbf{s}(\mathbf{x}_t|\mathbf{c}, t) = \nabla_{\mathbf{x}_t} \log p(\mathbf{x}_t|\mathbf{c})$ . Formally, we start with the log-density ratio between two nearby timesteps:

$$\log \frac{p_t(\mathbf{x}_t|\mathbf{c})}{p_{t+\delta(t)}(\mathbf{x}_t|\mathbf{c})} = \log p_t(\mathbf{x}_t|\mathbf{c}) - \log p_{t+\delta(t)}(\mathbf{x}_t|\mathbf{c}), \quad (4.2)$$

and take the gradient with respect to  $\mathbf{x}$  to obtain the score

difference:

$$\begin{aligned} \nabla_{\mathbf{x}} \log \frac{p_t(\mathbf{x}_t|\mathbf{c})}{p_{t+\delta(t)}(\mathbf{x}_t|\mathbf{c})} &= \nabla_{\mathbf{x}} \log p_t(\mathbf{x}_t|\mathbf{c}) - \nabla_{\mathbf{x}} \log p_{t+\delta(t)}(\mathbf{x}_t|\mathbf{c}) \\ &= \mathbf{s}(\mathbf{x}_t|\mathbf{c}, t) - \mathbf{s}(\mathbf{x}_t|\mathbf{c}, t + \delta(t)). \end{aligned} \quad (4.3)$$

Finally, the score with scale  $\omega$  can be written as:

$$\begin{aligned} \mathbf{s}^{SG}(\mathbf{x}_t|\mathbf{c}, t) &:= \mathbf{s}(\mathbf{x}_t|\mathbf{c}, t) \\ &+ \omega \left\{ \mathbf{s}(\mathbf{x}_t|\mathbf{c}, t) - \mathbf{s}(\mathbf{x}_t|\mathbf{c}, t + \delta(t)) \right\}, \end{aligned} \quad (4.4)$$

Fig. 3 illustrates how Self-Guidance is applied in practice at each denoising step during the reverse diffusion process. For a noisy latent  $\mathbf{x}_t$  at timestep  $t$ , the model simultaneously predicts the noise at  $t$  and at a noisier timestep  $t + \delta(t)$ . These two predictions are then linearly combined as in Eq. 4.4, and the combined prediction is subsequently used to denoise  $\mathbf{x}_t$  and obtain the latent  $\mathbf{x}_{t-1}$  for the next denoising step. This can be easily implemented by inference with the same model with two different timesteps within a batch. This means SG does not require an additional network or specific training tricks as in other guidance algorithms, but only uses the trained model itself. That is why we called the method **Self-Guidance**.

There are various choices of the shifted noise scale  $\delta(t)$ . In this paper, we consider a constant shift scale that is fixed independent of diffusion time  $t$ , and a dynamic one  $\delta(t) = t/\sigma$  that becomes smaller as  $t$  approaches 0. The latter allows a stronger Self-Guidance at the beginning of the diffusion sampling process. Moreover, we can also simply reuse the output distribution  $\mathbf{s}(\mathbf{x}_{t+1}|\mathbf{c}, t + 1)$  from the previous diffusion step to approximate the SG guidance term,

---

**Algorithm 1:** Diffusion model inference with Self-Guidance and other guidances

---

**Input:** Conditional DM  $d_{cod(\theta)}$ , Unconditional DM  $d_{uncod(\theta)}$ , Perturbed DM  $\hat{d}_{cod(\theta)}$ , guidance scales  $\omega_{CFG}, \omega_{PAG}, \omega_{SG}$ , shift scales  $\delta(t)$ .

```
for  $t$  in timesteps do
   $s(\mathbf{x}_t|\mathbf{c}, t) = d_{cod(\theta)}(\mathbf{x}_t, \mathbf{c}, t)$ 
  if Classifier-free guidance then
    |  $s(\mathbf{x}_t|t) = d_{uncod(\theta)}(\mathbf{x}_t, t)$ 
  end
  if Perturbed-attention guidance then
    |  $\hat{s}(\mathbf{x}_t|\mathbf{c}, t) = \hat{d}_{cod(\theta)}(\mathbf{x}_t, \mathbf{c}, t)$ 
  end
  if Self-Guidance then
    |  $s(\mathbf{x}_t|\mathbf{c}, t + \delta(t))$ 
    | =  $d_{cod(\theta)}(\mathbf{x}_t, \mathbf{c}, t + \delta(t))$  if SG
    |  $\approx d_{cod(\theta)}(\mathbf{x}_{t+1}, \mathbf{c}, t + 1)$  if SG-prev
  end
   $s^*(\mathbf{x}_t|\mathbf{c}, t) = s(\mathbf{x}_t|t)$ 
  |  $+ \omega_{CFG} * (s(\mathbf{x}_t|\mathbf{c}, t) - s(\mathbf{x}_t|t))$ 
  |  $+ \omega_{PAG} * (s(\mathbf{x}_t|\mathbf{c}, t) - \hat{s}(\mathbf{x}_t|\mathbf{c}, t))$ 
  |  $+ \omega_{SG} * (s(\mathbf{x}_t|\mathbf{c}, t) - s(\mathbf{x}_t|\mathbf{c}, t + \delta(t)))$ 
   $\mathbf{x}_{t-1} = \text{scheduler.step}(s^*(\mathbf{x}_t|\mathbf{c}, t), t, \mathbf{x}_t)$ 
end
return  $\mathbf{x}_0$ 
```

---

as in Eq. 4.5

$$s^{SG\_prev}(\mathbf{x}_t|\mathbf{c}, t) := s(\mathbf{x}_t|\mathbf{c}, t) + \omega \left\{ s(\mathbf{x}_t|\mathbf{c}, t) - s(\mathbf{x}_{t+1}|\mathbf{c}, t + 1) \right\}. \quad (4.5)$$

This avoids doubling inference time as it does not require an additional forward pass at each diffusion step. We call this approximation method **SG-prev**. In experiments, we will compare these choices in both Text-to-Image and Text-to-Video models.

We detail how SG and SG-prev are used in inference in Algorithm 1, as well as if combined with other diffusion guidance methods, such as CFG and PAG. For a single step at the noise level  $t$ , the diffusion model applies different guidance individually by forwarding the model with the corresponding settings: unconditional prediction in CFG, perturbing the attention in PAG, a shifted timestep  $t + \delta(t)$  in SG, and the previous timesteps output in SG-prev. These correct terms provide orthogonal improvements. Combined with their corresponding weight factors  $\omega_{CFG}, \omega_{PAG}, \omega_{SG}$ , the overall prediction is optimized to achieve higher consistency and control in the quality of the generation.

**Discussion** Suppressing artifacts with  $\frac{p_t(\mathbf{x}_t|\mathbf{c})}{p_{t+\delta(t)}(\mathbf{x}_t|\mathbf{c})}$  can be motivated from the heat equation. Specifically, under Gaus-

sian smoothing with kernel  $\mathcal{N}(0, \sigma^2)$ , the diffused density evolves as:

$$\begin{aligned} p_{t+\delta(t)}(x) &= \int p_t(y) \mathcal{N}(x; y, \sigma^2 \delta(t)) dy \\ &= (p_t * \mathcal{N}(0, \sigma^2))(x). \end{aligned} \quad (4.6)$$

Differentiating with respect to  $t$  yields the classical heat equation:

$$\partial_t p_t(x) = \frac{1}{2} g(t)^2 \Delta_x p_t(x), \quad (4.7)$$

where  $g(t)$  denotes the noise scaling function and  $\Delta_x$  is the Laplacian operator. Now, assume that an artifact resides at a location  $x_{\text{artifact}}$  in a low-density region of  $p_t(x)$ , i.e., a ‘‘valley.’’ Under the multivariate second-derivative test, the Hessian at this point is positive definite, implying

$$\Delta_x p_t(x_{\text{artifact}}) > 0. \quad (4.8)$$

Thus, the heat equation implies:

$$\partial_t p_t(x_{\text{artifact}}) > 0 \Rightarrow p_{t+\delta(t)}(x_{\text{artifact}}) > p_t(x_{\text{artifact}}) \quad (4.9)$$

when  $\delta(t)$  is sufficiently small.

In other words, forward diffusion causes density to flow into low-density artifact regions, increasing their mass. Therefore, comparing  $p_t$  to  $p_{t+\delta(t)}$  (via their ratio) effectively downweights these artifact regions and promotes sampling from the true data manifold.

## 5. Experiments

### 5.1. Implementation Details

**Models** We apply our Self-Guidance on current state-of-the-art text-to-image and text-to-video models. For text-to-image, we consider both a classic diffusion model, Stable Diffusion 1.4 [52], and current state-of-the-art flow-based models, Stable-Diffusion 3 series [2, 8] and Flux.1 [29]. For text-to-video, we consider CogVideoX-5B [67], an open-source video generation model trained with flow matching.

To facilitate a fair comparison, we consistently evaluate the model with the same number of steps in inference: DDIM Solver with 50 steps for SD 1.4, Euler with 28 steps for SD 3 series, and FLUX. The guidance scales for CFG and PAG are kept the same as the original settings in the corresponding papers. We will elaborate in Appendix C.3.

**Evaluation Metrics** We employ Fréchet Inception Distance (FID) [10], Human Preference Score (HPS v2.1) [64], CLIP Score [70], and Aesthetic Score[55] to comprehensively assess the quality of the image generation. For video generation, we employ VBench[19] to decompose video generation quality into multiple well-defined dimensions.

In addition, to address and analyze the performance on some long-standing problems in image generation, we introduce some specific evaluation metrics, including Hand-Conf [10, 47], Hand-FID (FID-H) [10] in hand generation,

Model	Approach	FID↓	HPS v2.1					Clip Score↑	Aesthetic Score↑
			concept-art↑	photo↑	anime↑	paintings↑	average↑		
SD 1.4[52]	baseline	50.76	21.22	21.24	21.37	20.52	21.09	0.2695	5.0025
	SG	42.73	22.13	22.23	21.84	21.73	21.98	0.2781	5.0766
	CFG[11]	27.07	23.61	24.91	23.60	24.83	24.24	0.3095	5.4427
	CFG+PAG[1]	27.37	23.61	24.87	24.86	23.73	24.26	0.3093	<b>5.4448</b>
	CFG+SG	26.67	<b>24.95</b>	25.17	24.13	24.12	24.59	0.3094	5.4201
	CFG+SG-prev	23.70	24.90	23.73	23.87	<b>25.10</b>	24.39	0.3110	5.2954
	CFG+PAG+SG	26.75	24.12	<b>25.28</b>	<b>24.99</b>	24.20	<b>24.65</b>	0.3094	5.4351
	CFG+PAG+SG-prev	<b>23.58</b>	23.94	25.17	24.91	23.75	24.44	<b>0.3115</b>	5.3444
SD 3[8]	baseline	51.47	21.17	18.91	21.11	21.62	20.70	0.2762	4.9628
	SG	48.82	22.01	19.49	20.79	21.47	20.83	0.2964	4.8888
	CFG[11]	27.00	30.26	28.29	30.81	30.62	30.00	0.3169	5.3915
	CFG+PAG[1]	27.34	30.26	28.45	30.78	30.73	30.05	0.3164	5.3978
	CFG+SG	25.21	<b>30.67</b>	28.49	<b>31.10</b>	<b>31.03</b>	30.32	0.3163	<b>5.4431</b>
	CFG+SG-prev	25.15	29.94	27.57	30.33	30.17	29.50	0.3217	5.3260
	CFG+PAG+SG	25.28	30.65	<b>28.72</b>	31.09	31.02	<b>30.37</b>	0.3162	5.4424
	CFG+PAG+SG-prev	<b>24.83</b>	29.92	27.79	30.34	30.26	29.58	<b>0.3219</b>	5.3238
SD 3.5[2]	baseline	39.69	22.06	22.98	23.87	22.03	22.74	0.3020	5.3068
	SG	38.40	23.74	24.74	25.08	23.39	24.24	0.3018	5.3986
	CFG[11]	23.86	31.67	29.48	<b>32.65</b>	31.43	31.31	0.3129	5.6152
	CFG+SG	22.70	<b>31.74</b>	<b>29.50</b>	32.57	<b>31.52</b>	<b>31.33</b>	0.3132	<b>5.6532</b>
	CFG+SG-prev	<b>20.74</b>	31.41	28.93	32.07	31.24	30.91	<b>0.3162</b>	5.6013
Flux.1[29]	CFG[11]	29.74	31.26	29.87	32.80	31.78	31.43	0.3080	5.7527
	CFG+SG	28.59	31.32	<b>30.02</b>	32.89	31.81	31.51	0.3084	<b>5.7845</b>
	CFG+SG-prev	<b>25.54</b>	<b>31.54</b>	29.71	<b>32.92</b>	<b>32.06</b>	<b>31.56</b>	<b>0.3129</b>	5.7391

Table 1. **Quantitative results of different Stable Diffusion models and Flux with various guidance.** FID, Clip Score and Aesthetic Score are evaluated on the MS-COCO 2017 validation subset. Bolded values highlight the best performance for each metric in each method.

Methods	Hand Generation		Face Generation		Text-Image Alignment	Generation Quality		
	FID-H ↓	Hand-Conf ↑	FID-F ↓	FaceScore ↑	CLIP Score ↑	FID ↓	Pick Score ↑	ImageReward ↑
Flux.1[29]	67.0163	0.9580	34.1976	4.5448	0.3080	29.74	22.9802	1.0971
+SG	<b>66.4360</b>	<b>0.9616</b>	<b>34.0561</b>	<b>4.6634</b>	<b>0.3084</b>	<b>28.59</b>	<b>22.9960</b>	<b>1.1046</b>

Table 2. **Quantitative results of SG Performances in Specific Generative Domains compared with CFG baseline Flux.1 [29].**

FaceScore[31], Face-FID (FID-F) [10] in face generation, Pick Score[27], ImageReward [65] in high-quality generation. We will elaborate on them in detail when used later.

## 5.2. Quantitative Comparisons

### 5.2.1. Text-to-Image Generation

Table 1 shows the effect of using SG itself on the three SD models. First of all, by incorporating SG itself on SD 1.4, we achieve an impressive 8-point (50.7602→**42.7362**) improvement in the FID. Similar improvements appear in other metrics and models as well. This indicates that SG itself is able to improve the quality of generated images.

SG is specifically designed to address the artifact issues in CFG and PAG. As shown in Table 1, incorporating SG with CFG leads to consistent improvements in HPS across all models, demonstrating that SG better aligns with human

preferences. Moreover, our approach remains competitive with PAG in both CLIP and Aesthetic Score.

Then, we find that combining SG with CFG and PAG will have the best performance over using them alone. In SD 1.4 and SD 3, this integration yields significant qualitative improvements, as detailed in the Appendix A.1. The results show that adding SG not only enhances fine-grained details, prompt alignment, and error correction but also achieves new SoTA better performance across multiple metrics (**24.65** HPS v2.1 for SD 1.4, **25.28** FID for SD 3, **0.3132** CLIP Score in SD 3.5, and **5.7845** Aesthetic Score in Flux).

In addition, it is surprising to find that SG-prev outperformed both compared baselines and the SG model, particularly in terms of FID and CLIP Score. This is achieved by applying SG-prev after the diffusion time (not step)  $t$  decreases below 500, because the earlier steps generate too

noisy images with clueless SG signals. This demonstrates that the SG-prev successfully boosts the diffusion models without incurring any additional cost.

### 5.2.2. Text-to-Video Generation

Table 3 provides quantitative evaluation results across four key dimensions in VBench [19]. The results indicate that adding SG effectively improves the metrics in human action (0.8320→**0.8450**), and multiple objects (0.4619→**0.4703**). SG-prev also outperforms the baseline across all four metrics under the same sampling time, but slightly lags behind SG that doubles sampling time. After having a close look at the generated examples in Figure 5, we find that SG also effectively eliminates artifact problems (broken arms and legs or misplaced limbs) in video generation tasks and enhances text-video consistency. Due to this comparison, we may conclude that SG is also effective in improving video generation quality. We will provide more video examples in Appendix A.2.

### 5.3. Guidance Performances in Specific Domains

Through our experiments and analysis (e.g. Figure 2), we observed that SG is particularly effective when handling some long-standing problems in image generation. More specifically, SG can effectively generate hands with an exact correct number of fingers with natural shapes (Part 1), and remove artifacts like redundant arms or hands (Part 2). It also enhances Flux’s comprehension of textual input (Part 4), effectively eliminating extraneous objects. This allows the main subject of the image to stand out while the background is appropriately blurred (Part 3).

To quantitatively reveal the effectiveness of SG in these aspects, we propose some domain-specific metrics and conduct a comparison with Flux.1 [29], the state-of-the-art text-to-image model. Here we introduce the metrics in detail.

**Hand Generation** To evaluate the quality of the hands in the generated images, we propose two metrics, the Fréchet Inception Distance for hands (FID-H) and the HAND-CONF. FID-H selects 5,000 human-hand-related prompts from the coco validation set, and calculates the distance between the generated image and the real images in COCO. To compute HAND-CONF, we detect hands on the generated images with a pretrained hand detector (i.e. Mediapipe [69]), and average the confidence scores on 5,000 prompts in the HandCaption-58k dataset [43].

**Face Generation** Fréchet Inception Distance for Faces (FID-F) is calculated with 5,000 face-related prompts and images in COCO val. Regarding FaceScore, we use a face quality-focused reward model [31] to score 10,000 images generated with prompts from the HumanCaption-10M dataset [46].

Moreover, to assess text-image consistency, we measured the CLIP Score. FID, PickScore [27] and ImageReward [65] are also listed here for general image quality assessments.

As shown in Table 2, SG achieves significant results in fine-grained generation tasks, such as hand and face generation, with improvements in FID-H (67.0163 to **66.4360**) and FID-F (34.1976 to **34.0561**). Additionally, the increase in PickScore and ImageReward indicates that our SG is more adept at producing higher-quality samples, thus minimizing generation errors, as illustrated in Part 4 of Figure 2.

In summary, our SG improves diffusion and flow-based models in multiple aspects, generating high-quality images.

### 5.4. Ablation Studies

#### 5.4.1. Guidance Scale

We conducted an experimental investigation into the effect of the guidance scale on the performance of Self-Guidance. Using Stable Diffusion 1.4 [52], we sampled 5000 images with guidance scales ranging from 0.0 to 5.0 in 1.0 intervals. We measure the FID [10] and HPS v2.1 [64] for these images. The results, as shown in Figure 6, indicate that Self-Guidance achieves the best FID (42.23) at a guidance scale of 2.0, and the highest HPS (21.98) at 3.0.

#### 5.4.2. Shift Scale

**Constant Shift Scale** The shift scale  $\delta(t)$  represents the extent to which the noise level deviates from the current level. A simple way is to set it to a constant independent of  $t$ . The larger the shift scale is, the more it could contrast with the current noise level to suppress the artifacts. However, too large shift may damage the desired patterns that should be preserved in the current sampling density, and thus a suitable shift scale should be adopted. Figure 6 shows how the FID and HPS score change as the shift scale increases from 0 to 50 (within 1,000 total training timesteps). According to the results, SG achieves the lowest FID and highest HPS score with the shift scale set to 30.

**Dynamic Shift Scale** One can also dynamically adjust  $\delta(t)$  during the reverse diffusion process. At higher noise levels, a large shift of  $\delta(t)$  can be adopted, as noisy artifacts can be rapidly removed at the early stage of diffusion sampling. Thus, we introduce  $\delta(t)$  as a linear function of time ( $\delta(t) = t/\sigma$ ), allowing stronger guidance at higher noise levels while reducing it at lower levels. More experiment results are shown in the Appendix A.4. We find that dynamic shift scaling improves quality, avoiding blurred images or noise issues caused by excessive guidance as the noise level decreases to zero.

### 6. Conclusions and Limitations

This paper suggests that the reason for artifacts in image generation is incompetent denoising at each step, and proposes Self-Guidance (SG), an inference-guidance strategy

**Prompt:** “A Samoyed and a Golden Retriever dog are playfully romping through a futuristic neon city at night. The neon lights emitted from the nearby buildings glistens off of their fur.”

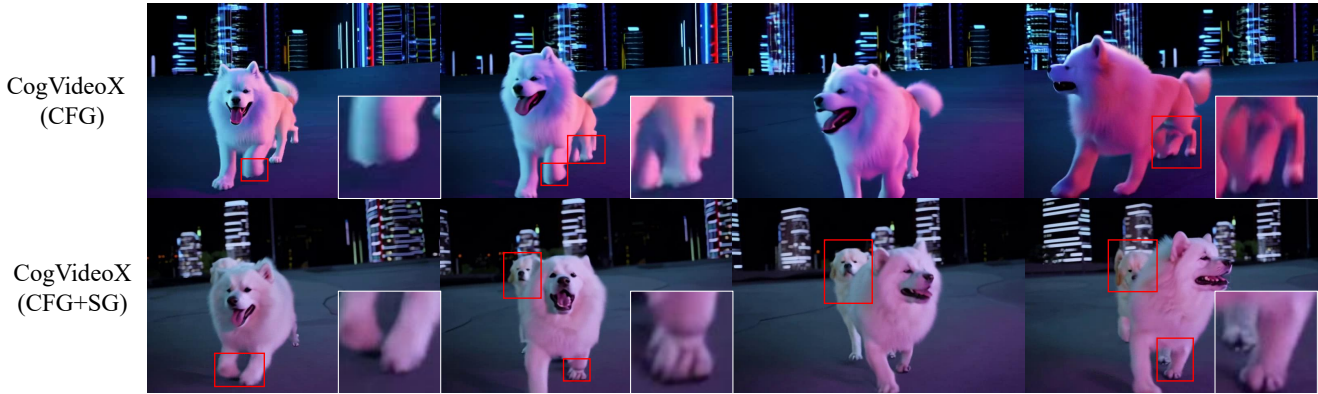


Figure 5. **Qualitative comparison between CFG and CFG+SG in text-to-video model CogVideoX-5B**[67]. The red box in the figure indicates where the baseline(CFG) is poorly generated, and the zoomed-in image is shown in the lower left corner. Adding SG to CFG effectively eliminates artifacts (Broken arms and legs and misplaced limbs) in video generation. SG also enhances the consistency between prompt and video(Number of dogs in the video).

Model	Human Action $\uparrow$	Overall Consistency $\uparrow$	Multiple Objects $\uparrow$	Appearance Style $\uparrow$
CogVideoX-5B[67]	0.8320	0.2526	0.4619	0.2331
+ SG	<b>0.8450</b>	<b>0.2553</b>	0.4703	<b>0.2339</b>
+SG-prev	0.8376	0.2530	<b>0.4774</b>	0.2333

Table 3. **Quantitative results of CFG based text-to-video generation model CogVideoX with our SG and SG-prev.** All scores are evaluated on the Standard Prompt Suite of VBench[19]. Bolded values highlight the best performance for each metric.

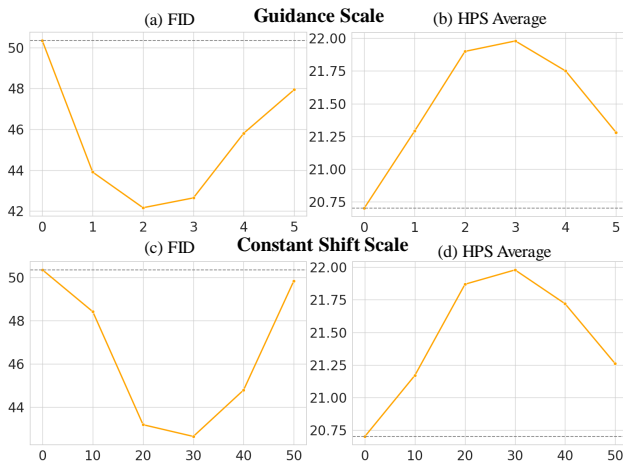


Figure 6. **Ablation study of the Guidance Scale and Shift Scale.**

to modulate the output distribution at each denoising step via incorporating the difference between the output probability distributions computed at both current time  $t$  and a noisier one  $t + \delta(t)$ . SG has multiple advantages, such as architecture independence, requiring no specific training, and compatibility with other well-established guidance methods. Intensive experiment results demonstrate that SG can consis-

tently improve generation performances on multiple popular text-to-image and text-to-video models, particularly effective when addressing long-standing problems like generating high-quality human hands and bodies.

While SG requires two forward passes per sampling step, it leads to increased computational cost. To address this issue, we propose an efficient method, SG-prev, which approximates SG by directly reusing the output from the immediately previous timestep. As a result, SG-prev introduces no additional computational cost.

## References

- [1] Donghoon Ahn, Hyoungwon Cho, Jaewon Min, Wooseok Jang, Jungwoo Kim, SeonHwa Kim, Hyun Hee Park, Kyong Hwan Jin, and Seungryong Kim. Self-rectifying diffusion sampling with perturbed-attention guidance, 2024. 1, 2, 3, 7
- [2] Stability AI. Introducing stable diffusion 3.5, 2023. Accessed: 2024-10-30. 1, 6, 7
- [3] Sina Alemohammad, Ahmed Intiaz Humayun, Shruti Agarwal, John Collomosse, and Richard Baraniuk. Self-improving diffusion models with synthetic data, 2024. 4
- [4] Andreas Blattmann, Tim Dockhorn, Sumith Kulal, Daniel Mendelevitch, Maciej Kilian, Dominik Lorenz, Yam Levi, Zion English, Vikram Voleti, Adam Letts, Varun Jampani,

- and Robin Rombach. Stable video diffusion: Scaling latent video diffusion models to large datasets, 2023. 1
- [5] Ricky TQ Chen, Jens Behrmann, David K Duvenaud, and Jörn-Henrik Jacobsen. Residual flows for invertible generative modeling. In *Advances in Neural Information Processing Systems*, pages 9916–9926, 2019. 1
- [6] Guillaume Couairon, Jakob Verbeek, Holger Schwenk, and Matthieu Cord. Diffedit: Diffusion-based semantic image editing with mask guidance. *ArXiv*, abs/2210.11427, 2022. 1
- [7] Wei Deng, Weijian Luo, Yixin Tan, Marin Bilos, Yu Chen, Yuriy Nevmyvaka, and Ricky TQ Chen. Variational schrödinger diffusion models. *arXiv preprint arXiv:2405.04795*, 2024. 1
- [8] Patrick Esser, Sumith Kulal, Andreas Blattmann, Rahim Entezari, Jonas Müller, Harry Saini, Yam Levi, Dominik Lorenz, Axel Sauer, Frederic Boesel, Dustin Podell, Tim Dockhorn, Zion English, Kyle Lacey, Alex Goodwin, Yannik Marek, and Robin Rombach. Scaling rectified flow transformers for high-resolution image synthesis, 2024. 1, 2, 6, 7
- [9] Zhengyang Geng, Ashwini Pople, William Luo, Justin Lin, and J Zico Kolter. Consistency models made easy. *arXiv preprint arXiv:2406.14548*, 2024. 1
- [10] Martin Heusel, Hubert Ramsauer, Thomas Unterthiner, Bernhard Nessler, and Sepp Hochreiter. Gans trained by a two time-scale update rule converge to a local nash equilibrium, 2018. 2, 6, 7, 8
- [11] Jonathan Ho and Tim Salimans. Classifier-free diffusion guidance, 2022. 1, 2, 3, 4, 7
- [12] Jonathan Ho, Ajay Jain, and Pieter Abbeel. Denoising diffusion probabilistic models. *Advances in Neural Information Processing Systems*, 33:6840–6851, 2020. 1
- [13] Jonathan Ho, Ajay Jain, and Pieter Abbeel. Denoising diffusion probabilistic models. *Advances in Neural Information Processing Systems*, 33:6840–6851, 2020. 4
- [14] Jonathan Ho, Tim Salimans, Alexey Gritsenko, William Chan, Mohammad Norouzi, and David J Fleet. Video diffusion models. *arXiv preprint arXiv:2204.03458*, 2022. 1
- [15] Susung Hong. Smoothed energy guidance: Guiding diffusion models with reduced energy curvature of attention, 2024. 4
- [16] Susung Hong, Gyuseong Lee, Wooseok Jang, and Seungryong Kim. Improving sample quality of diffusion models using self-attention guidance, 2023. 1, 3
- [17] Emiel Hoogeboom, Victor Garcia Satorras, Clément Vignac, and Max Welling. Equivariant diffusion for molecule generation in 3d. In *International Conference on Machine Learning*, pages 8867–8887. PMLR, 2022. 1
- [18] Xinyu Huang, Youcai Zhang, Jinyu Ma, Weiwei Tian, Rui Feng, Yuejie Zhang, Yaqian Li, Yandong Guo, and Lei Zhang. Tag2text: Guiding vision-language model via image tagging, 2024. 4
- [19] Ziqi Huang, Yanan He, Jiashuo Yu, Fan Zhang, Chenyang Si, Yuming Jiang, Yuanhan Zhang, Tianxing Wu, Qingyang Jin, Nattapol Chanpaisit, Yaohui Wang, Xinyuan Chen, Limin Wang, Dahua Lin, Yu Qiao, and Ziwei Liu. Vbench: Comprehensive benchmark suite for video generative models, 2023. 6, 8, 9, 3
- [20] Zemin Huang, Zhengyang Geng, Weijian Luo, and Guojun Qi. Flow generator matching. *arXiv preprint arXiv:2410.19310*, 2024. 1
- [21] Tero Karras, Samuli Laine, Miika Aittala, Janne Hellsten, Jaakko Lehtinen, and Timo Aila. Analyzing and improving the image quality of stylegan. In *Proceedings of the IEEE/CVF conference on computer vision and pattern recognition*, pages 8110–8119, 2020. 1
- [22] Tero Karras, Miika Aittala, Timo Aila, and Samuli Laine. Elucidating the design space of diffusion-based generative models. In *Proc. NeurIPS*, 2022. 1
- [23] Tero Karras, Miika Aittala, Tuomas Kynkäänniemi, Jaakko Lehtinen, Timo Aila, and Samuli Laine. Guiding a diffusion model with a bad version of itself, 2024. 2, 3
- [24] Tero Karras, Miika Aittala, Jaakko Lehtinen, Janne Hellsten, Timo Aila, and Samuli Laine. Analyzing and improving the training dynamics of diffusion models, 2024. 3
- [25] Heeseung Kim, Sungwon Kim, and Sungroh Yoon. Guided-tts: A diffusion model for text-to-speech via classifier guidance. In *International Conference on Machine Learning*, pages 11119–11133. PMLR, 2022. 1
- [26] Diederik P. Kingma and Prafulla Dhariwal. Glow: Generative flow with invertible 1x1 convolutions, 2018. 1
- [27] Yuval Kirstain, Adam Polyak, Uriel Singer, Shahbuland Matiana, Joe Penna, and Omer Levy. Pick-a-pic: An open dataset of user preferences for text-to-image generation, 2023. 7, 8
- [28] Zhifeng Kong, Wei Ping, Jiayi Huang, Kexin Zhao, and Bryan Catanzaro. Diffwave: A versatile diffusion model for audio synthesis. In *International Conference on Learning Representations*, 2020. 1
- [29] Black Forest Labs. Flux.1, 2023. 1, 2, 6, 7, 8
- [30] Kunchang Li, Yali Wang, Yizhuo Li, Yi Wang, Yanan He, Limin Wang, and Yu Qiao. Unmasked teacher: Towards training-efficient video foundation models. In *Proceedings of the IEEE/CVF International Conference on Computer Vision*, pages 19948–19960, 2023. 4
- [31] Zhenyi Liao, Qingsong Xie, Chen Chen, Hannan Lu, and Zhijie Deng. Facescore: Benchmarking and enhancing face quality in human generation, 2024. 7, 8
- [32] Yaron Lipman, Ricky T. Q. Chen, Heli Ben-Hamu, Maximilian Nickel, and Matt Le. Flow matching for generative modeling. *ArXiv*, abs/2210.02747, 2022. 4
- [33] Luping Liu, Yi Ren, Zhijie Lin, and Zhou Zhao. Pseudo numerical methods for diffusion models on manifolds. *arXiv preprint arXiv:2202.09778*, 2022. 3
- [34] Xingchao Liu, Chengyue Gong, and Qiang Liu. Flow straight and fast: Learning to generate and transfer data with rectified flow. *arXiv preprint arXiv:2209.03003*, 2022. 4
- [35] Cheng Lu, Yuhao Zhou, Fan Bao, Jianfei Chen, Chongxuan Li, and Jun Zhu. Dpm-solver: A fast ode solver for diffusion probabilistic model sampling in around 10 steps. *arXiv preprint arXiv:2206.00927*, 2022. 3
- [36] Weijian Luo. Diff-instruct++: Training one-step text-to-image generator model to align with human preferences. *arXiv preprint arXiv:2410.18881*, 2024. 1
- [37] Weijian Luo, Tianyang Hu, Shifeng Zhang, Jiacheng Sun, Zhenguo Li, and Zhihua Zhang. Diff-instruct: A universal approach for transferring knowledge from pre-trained diffusion

- models. *Advances in Neural Information Processing Systems*, 36, 2024.
- [38] Weijian Luo, Zemin Huang, Zhengyang Geng, J Zico Kolter, and Guo-jun Qi. One-step diffusion distillation through score implicit matching. *arXiv preprint arXiv:2410.16794*, 2024. 1
- [39] Weijian Luo, Boya Zhang, and Zihua Zhang. Entropy-based training methods for scalable neural implicit samplers. *Advances in Neural Information Processing Systems*, 36, 2024. 1
- [40] Weijian Luo, Colin Zhang, Debing Zhang, and Zhengyang Geng. Diff-instruct\*: Towards human-preferred one-step text-to-image generative models. *arXiv preprint arXiv:2410.20898*, 2024. 1
- [41] Yang Luo, Yiheng Zhang, Zhaofan Qiu, Ting Yao, Zhineng Chen, Yu-Gang Jiang, and Tao Mei. Freenhance: Tuning-free image enhancement via content-consistent noising-and-denoising process. In *Proceedings of the 32nd ACM International Conference on Multimedia*, page 7075–7084, New York, NY, USA, 2024. Association for Computing Machinery. 4
- [42] Chenlin Meng, Yang Song, Jiaming Song, Jiajun Wu, Jun-Yan Zhu, and Stefano Ermon. Sdedit: Image synthesis and editing with stochastic differential equations. *arXiv preprint arXiv:2108.01073*, 2021. 1
- [43] Nagolinc. Hand captions, 2023. Accessed: 2024-10-31. 8
- [44] Alex Nichol and Prafulla Dhariwal. Improved denoising diffusion probabilistic models. *arXiv preprint arXiv:2102.09672*, 2021. 1
- [45] Aaron van den Oord, Sander Dieleman, Heiga Zen, Karen Simonyan, Oriol Vinyals, Alex Graves, Nal Kalchbrenner, Andrew Senior, and Koray Kavukcuoglu. Wavenet: A generative model for raw audio. *arXiv preprint arXiv:1609.03499*, 2016. 1
- [46] OpenFace and CQUPT. Humancaption-10m, 2023. Accessed: 2024-10-31. 8
- [47] Gaurav Parmar, Richard Zhang, and Jun-Yan Zhu. On aliased resizing and surprising subtleties in gan evaluation, 2022. 6
- [48] Ben Poole, Ajay Jain, Jonathan T Barron, and Ben Mildenhall. Dreamfusion: Text-to-3d using 2d diffusion. *arXiv preprint arXiv:2209.14988*, 2022. 1
- [49] Alec Radford, Jong Wook Kim, Chris Hallacy, Aditya Ramesh, Gabriel Goh, Sandhini Agarwal, Girish Sastry, Amanda Askell, Pamela Mishkin, Jack Clark, et al. Learning transferable visual models from natural language supervision. In *International conference on machine learning*, pages 8748–8763. PMLR, 2021. 4
- [50] Aditya Ramesh, Mikhail Pavlov, Gabriel Goh, Scott Gray, Chelsea Voss, Alec Radford, Mark Chen, and Ilya Sutskever. Zero-shot text-to-image generation. In *International Conference on Machine Learning*, pages 8821–8831. PMLR, 2021. 1
- [51] Aditya Ramesh, Prafulla Dhariwal, Alex Nichol, Casey Chu, and Mark Chen. Hierarchical text-conditional image generation with clip latents. *arXiv preprint arXiv:2204.06125*, 2022. 1
- [52] Robin Rombach, Andreas Blattmann, Dominik Lorenz, Patrick Esser, and Björn Ommer. High-resolution image synthesis with latent diffusion models. In *Proceedings of the IEEE/CVF Conference on Computer Vision and Pattern Recognition*, pages 10684–10695, 2022. 2, 4, 6, 7, 8
- [53] Seyedmorteza Sadat, Manuel Kansy, Otmar Hilliges, and Romann M. Weber. No training, no problem: Rethinking classifier-free guidance for diffusion models, 2024. 3
- [54] Chitwan Saharia, William Chan, Saurabh Saxena, Lala Li, Jay Whang, Emily Denton, Seyed Kamyar Seyed Ghasemipour, Burcu Karagol Ayan, S Sara Mahdavi, Rapha Gontijo Lopes, et al. Photorealistic text-to-image diffusion models with deep language understanding. *arXiv preprint arXiv:2205.11487*, 2022. 1
- [55] Christoph Schuhmann. Improved aesthetic predictor, 2023. 6, 3
- [56] Shuai Shen, Wenliang Zhao, Zibin Meng, Wanhua Li, Zheng Zhu, Jie Zhou, and Jiwen Lu. Diftalk: Crafting diffusion models for generalized audio-driven portraits animation, 2023. 1
- [57] Jascha Sohl-Dickstein, Peter Battaglino, and Michael R DeWeese. Minimum probability flow learning. *arXiv preprint arXiv:0906.4779*, 2009. 4
- [58] Jiaming Song, Chenlin Meng, and Stefano Ermon. Denoising diffusion implicit models. *arXiv preprint arXiv:2010.02502*, 2020. 1
- [59] Yang Song, Jascha Sohl-Dickstein, Diederik P Kingma, Abhishek Kumar, Stefano Ermon, and Ben Poole. Score-based generative modeling through stochastic differential equations. In *International Conference on Learning Representations*, 2020. 4
- [60] Yang Song, Conor Durkan, Iain Murray, and Stefano Ermon. Maximum likelihood training of score-based diffusion models. *Advances in Neural Information Processing Systems*, 34:1415–1428, 2021. 1
- [61] Pascal Vincent. A Connection Between Score Matching and Denoising Autoencoders. *Neural Computation*, 23(7):1661–1674, 2011. 4
- [62] Yifei Wang, Weimin Bai, Weijian Luo, Wenzheng Chen, and He Sun. Integrating amortized inference with diffusion models for learning clean distribution from corrupted images. *arXiv preprint arXiv:2407.11162*, 2024. 1
- [63] Yi Wang, Yanan He, Yizhuo Li, Kunchang Li, Jiashuo Yu, Xin Ma, Xinhao Li, Guo Chen, Xinyuan Chen, Yaohui Wang, Conghui He, Ping Luo, Ziwei Liu, Yali Wang, Limin Wang, and Yu Qiao. Internvid: A large-scale video-text dataset for multimodal understanding and generation, 2024. 4
- [64] Xiaoshi Wu, Yiming Hao, Keqiang Sun, Yixiong Chen, Feng Zhu, Rui Zhao, and Hongsheng Li. Human preference score v2: A solid benchmark for evaluating human preferences of text-to-image synthesis, 2023. 2, 6, 8, 3
- [65] Jiazheng Xu, Xiao Liu, Yuchen Wu, Yuxuan Tong, Qinkai Li, Ming Ding, Jie Tang, and Yuxiao Dong. Imagereward: Learning and evaluating human preferences for text-to-image generation, 2023. 7, 8
- [66] Shuchen Xue, Mingyang Yi, Weijian Luo, Shifeng Zhang, Jiacheng Sun, Zhenguo Li, and Zhi-Ming Ma. Sa-solver: Stochastic adams solver for fast sampling of diffusion models. *Advances in Neural Information Processing Systems*, 36, 2024. 3

- [67] Zhuoyi Yang, Jiayan Teng, Wendi Zheng, Ming Ding, Shiyu Huang, Jiazheng Xu, Yuanming Yang, Wenyi Hong, Xiaohan Zhang, Guanyu Feng, Da Yin, Xiaotao Gu, Yuxuan Zhang, Weihang Wang, Yean Cheng, Ting Liu, Bin Xu, Yuxiao Dong, and Jie Tang. Cogvideox: Text-to-video diffusion models with an expert transformer, 2024. [1](#), [2](#), [6](#), [9](#)
- [68] Boya Zhang, Weijian Luo, and Zhihua Zhang. Enhancing adversarial robustness via score-based optimization. *Advances in Neural Information Processing Systems*, 36:51810–51829, 2023. [1](#)
- [69] Fan Zhang, Valentin Bazarevsky, Andrey Vakunov, Andrei Tkachenka, George Sung, Chuo-Ling Chang, and Matthias Grundmann. Mediapipe hands: On-device real-time hand tracking, 2020. [8](#)
- [70] SUN Zhengwentai. clip-score: CLIP Score for PyTorch. <https://github.com/taited/clip-score>, 2023. Version 0.1.1. [6](#), [3](#)

# Self-Guidance: Boosting Flow and Diffusion Generation on Their Own

## Supplementary Material

### A. Additional results

#### A.1. More results of SG combining with CFG and PAG

Figure 8 shows the comparison between CFG, CFG+PAG, and CFG + PAG+SG. The results show that adding SG to CFG and PAG significantly enhances the model’s ability to generate fine details (e.g., hands are rendered more realistically), and improves prompt alignment, ensuring generated images better match the intended descriptions. SG also effectively corrects errors seen in previous samples, such as extra hands or incorrect body configurations in humans and animals.

#### A.2. More results of Text-to-Video Generation

Figure 10 shows more results of our SG on Test-to-Video models, similar to Figure 5. For complete video examples, see the videos folder of the Appendix.

#### A.3. More results of ablations of guidance scale and shift scale

Figure 7 shows the results of different guidance scales and shift scales on Stable Diffusion 3-medium. We can find that with the increase of the guidance scale and shift scale, our SG can significantly improve the guidance performance.

#### A.4. More results of ablations of dynamic shift scale

Figure 9 shows the result of the dynamic shift scale on the EDM2-XXL model.  $\sigma$  is a fixed value. We let the shift scale  $\delta(t)$  be  $-\sigma$ ,  $\sigma$ , and  $t/\sigma$ . The results show that using fixed  $\delta(t)$  caused either blurred images or excessive noise, while dynamic  $\delta(t)$  is better.

### B. Details of the flow models

#### B.1. Flow Matching (FM)

Flow Matching (FM) is based on continuous normalizing flows, where the generative model is defined as an ordinary differential equation (ODE):

$$\frac{dz_t}{dt} = v(z_t, t) \quad (\text{B.1})$$

Here,  $t \in [0, 1]$ , and  $v(z_t, t)$  is referred to as the vector field. This ODE defines a probability path  $p_t$ , transitioning from a noise distribution  $p_1$  to the data distribution  $p_0$ . Once  $v(z_t, t)$  is known, we can use an ODE solver to generate data samples.

The vector field  $v_\theta(z_t, t)$  is parameterized by a neural network, and the FM objective is:

$$L_{FM} = \mathbb{E}_{t, p_t(z)} \|v_\theta(z, t) - u_t(z)\|_2^2 \quad (\text{B.2})$$

Here,  $u_t(z)$  is the target vector field, defining the probability path  $p_t(z)$  from  $p_1$  to  $p_0$ . Without priors,  $u_t(z)$  is unknown. FM introduces a predefined  $u_t(z)$  using a conditional probability path  $p_t(z|x_0)$ , where  $x_0$  is the real data. This is modeled as:

$$p_t(z|x_0) = \mathcal{N}(z|a_t x_0, b_t^2 I) \quad (\text{B.3})$$

Here,  $a_t$  and  $b_t$  are time-dependent functions. If  $a_0 = 1, b_0 = 0$ , then  $p_0(z|x_0) = q(x_0)$ , and if  $a_1 = 0, b_1 = 1$ , then  $p_1(z|x_0) = p_1$ . This aligns with the diffusion process  $z_t = a_t x_0 + b_t \epsilon$ , where  $\epsilon \sim \mathcal{N}(0, I)$ .

#### B.2. Conditional Flow Matching (CFM)

The Conditional Flow Matching (CFM) objective is:

$$L_{CFM} = \mathbb{E}_{t, q(x_0), p_t(z|x_0)} \|v_\theta(z, t) - u_t(z|x_0)\|_2^2 \quad (\text{B.4})$$

Here,  $u_t(z|x_0)$  defines the conditional probability path  $p_t(z|x_0)$ . It can be derived as:

$$u_t(z|x_0) = \frac{a'_t}{a_t} z_t - b_t^2 \lambda'_t \epsilon \quad (\text{B.5})$$

where  $\lambda_t = \log \frac{a^2}{b^2}$  is the Signal-to-Noise Ratio(SNR), then we can get  $\lambda'_t = 2 \left( \frac{a'_t}{a_t} - \frac{b'_t}{b_t} \right)$ . The final CFM objective becomes:

$$L_{CFM} = \mathbb{E}_{t, q(x_0), p_t(z|x_0), \epsilon \sim \mathcal{N}(0, I)} \left\| v_\theta(z, t) - \left( \frac{a'_t}{a_t} z_t - b_t^2 \lambda'_t \epsilon \right) \right\|_2^2 \quad (\text{B.6})$$

By defining  $v_\theta(z, t) = \frac{a'_t}{a_t} z_t - b_t^2 \lambda'_t \epsilon_\theta(z, t)$ , this becomes equivalent to noise prediction like DDPM, with an additional weight term.

#### B.3. Rectified Flow (RF)

RF simplifies the forward process to:

$$z_t = (1 - t)x_0 + t\epsilon$$

This linear interpolation allows larger step sizes during sampling. Its loss is straightforward:

$$L_{RF} = \mathbb{E}_{t, q(x_0), p_t(z|x_0), \epsilon \sim \mathcal{N}(0, I)} \|v_\theta(z, t) - (\epsilon - x_0)\|_2^2$$

For RF,  $w_t = \frac{t}{1-t}$ , showing its connection to FM and other diffusion models.



Figure 7. SG results of different guidance scales and shift scales on Stable Diffusion 3-medium.

## C. Implementation details

All experiments are conducted on NVIDIA GeForce RTX V100 GPU and NVIDIA RTX A100 GPU for image and video sampling. We obtain all the necessary weights from publicly available repositories.

### C.1. Metrics for Text-to-Image Generation

To evaluate the performance of Text-to-Image models, we employed several metrics:

- **Fréchet Inception Distance (FID)** [10] quantifies the similarity between generated images and real images.



Figure 8. **Qualitative comparison between CFG, CFG+PAG and CFG + PAG+SG.** The red box in the figure indicates where the baseline (SD1.4 and SD3) is poorly generated, and the zoomed-in image is shown in the lower left corner.

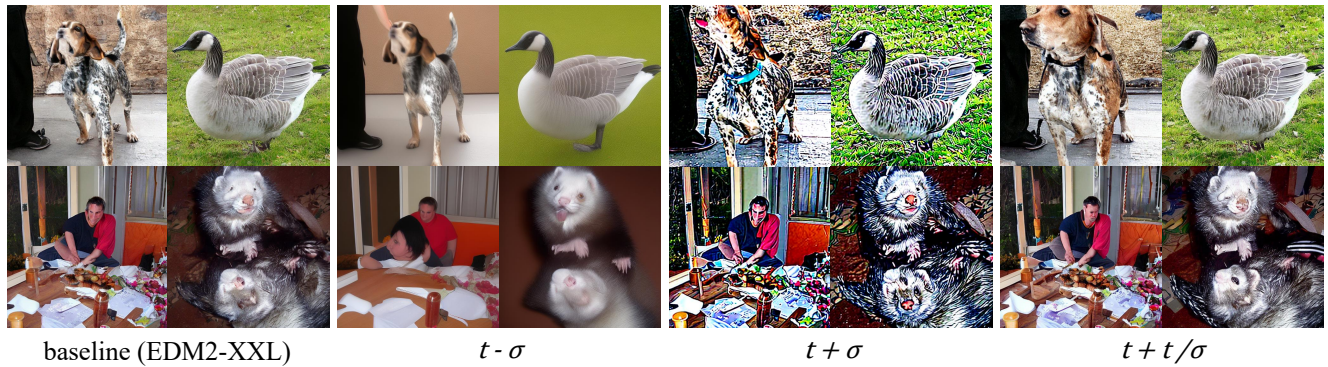


Figure 9. Ablation study of the dynamic shift scale on EDM2-XXL[24].

- **Human Preference Score (HPS v2.1)** [64] assesses the quality of generated images based on human judgment.
- **CLIP Score** [70] measures the alignment between generated images and their textual descriptions.
- **Aesthetic Score** [55] evaluates the visual quality and appeal of the images.

FID, CLIP Score, and Aesthetic Score were conducted using 5000 prompts in the MS-COCO 2017 validation dataset.

HPS v2.1 used the standard prompts they provided.

## C.2. Metrics for Text-to-Video Generation

To evaluate the performance of Text-to-Video models, we utilized VBench[19], a comprehensive benchmark specifically designed for video generative. We evaluate model performance across five key dimensions: human action, scene, multiple objects, appearance style, and overall consistency.

**Prompt:** “A dynamic video of a person walking through a vibrant city at night, with colorful neon lights reflecting off wet streets. The person, dressed in futuristic attire, moves through bustling crowds, with the camera follow”



**Prompt:** “A stylish woman walks down a Tokyo street filled with warm glowing neon and animated city signage. She wears a black leather jacket, a long red dress, and black boots, and carries a black purse. ”



Figure 10. Additional results for using SG on Text-to-Video models, similar to Figure 5

	Stable-Diffusion 1.4	Stable-Diffusion 3-Medium	Stable-Diffusion 3.5-Large	Flux.1-dev
CFG guidance scale	7.5	3.5	3.5	3.5
PAG guidance scale	0.3	0.7	-	-
SG guidance scale	3	3	3	3
SG constant shift scale	10	10	10	10

Table 4. The parameters of CFG, PAG, and SG used during inference for four diffusion models.

- **Human Action:** Use UMT [30] to assess if generated videos accurately depict the specific actions described in text prompts.
- **Scene:** Use Tag2Text [18] to caption generated scenes and verify their consistency with the text prompt (e.g., "ocean" vs. "river").
- **Multiple Objects:** Evaluate the success rate of generating all objects specified in the text prompt within each video frame.
- **Appearance Style:** Use CLIP [49] to feature similarity between frames and style descriptions (e.g., "oil painting" or "cyberpunk").

- **Overall Consistency:** Use ViCLIP [63] to calculate overall video-text consistency, reflecting semantic and style alignment.

### C.3. Guidance Scale Setting

The guidance scales for CFG and PAG are kept the same as the original settings in corresponding papers. For each diffusion model, we provide the best guidance scale and constant shift scale of Self-Guidance. The specific parameters for these three guidance methods are in Table 4.